A&A manuscript no.
(will be inserted by hand later)

Your thesaurus codes are:
05 (05.01.1; 03.20.2; 11.17.4 QSO 1150+812; 11.02.2 BL 1803+784)

ASTRONOMY AND ASTROPHYSICS
May 31, 2000

Towards global phase-delay VLBI astrometry: Observations of QSO 1150+812 and BL 1803+784

M.A. Pérez-Torres[1] ⋆, J.M. Marcaide[1], J.C. Guirado[1], E. Ros[2], I.I. Shapiro[3], M.I. Ratner[3], and E. Sardón[4]

[1] Departamento de Astronomía y Astrofísica, Universidad de Valencia, E-46100 Burjassot, Valencia, Spain
[2] Max-Planck-Institut für Radioastronomie, Auf dem Hügel 69, D-53121, Bonn, Germany
[3] Harvard-Smithsonian Center for Astrophysics, Cambridge, MA 02138, USA
[4] Grupo de Mecánica de Vuelos, Isaac Newton 11, E-28760 Tres Cantos, Madrid, Spain

Received 21 March 2000/ Accepted 25 May 2000

Abstract. On 18 November 1993, we observed the QSO 1150+812 and the BL Lac object 1803+784, nearly 15° apart on the sky, with a VLBI array, simultaneously recording at 8.4 and 2.3 GHz. Using difference astrometry techniques, we determined the coordinates of 1803+784 relative to those of 1150+812 to be

$$\Delta\alpha = 6^h\,7^m\,33\overset{s}{.}18469 \pm 0\overset{s}{.}00020$$
$$\Delta\delta = -2^\circ\,30'\,25\overset{''}{.}13557 \pm 0\overset{''}{.}00075$$

These standard errors contain estimated contributions from the propagation medium, the effects of source opacity, and the possible misidentification of the reference point in some of the maps. We obtained comparably accurate and consistent relative positions of the radio sources with GPS-based ionosphere corrections, thus demonstrating that dual-frequency observations are not required for state-of-the-art accuracy in VLBI astrometry. These results also demonstrate the feasibility of using single-frequency measurements for sources separated by 15° on the sky, and open the avenue for the application of this technique on a full-sky scale.

Key words: astrometry – techniques: interferometric – quasars: individual: 1150+812 – BL Lac: individual: 1803+784

1. Introduction

The establishment of a radio reference frame with sub-milliarcsecond accuracy has been a major goal of astrometrists for the last several decades. Centimeter-wavelength very-long-baseline interferometry (VLBI) group-delay astrometry of extragalactic radio sources routinely provides precisions at the milliarcsecond (mas) level, thus allowing a celestial reference frame to be built with corresponding accuracy (e.g., Ma et al. 1998). The use of phase-delay difference astrometry (see, e.g., Shapiro et al. 1979) allows us to determine angular separations between pairs of radio sources at the submilliarcsecond level. One important advantage of phase-delay astrometry is that we can identify with sufficient accuracy suitable reference points within the structures of the radio sources whose relative positions we wish to determine, whereas in group-delay astrometry suitable reference points are not so easily identified from epoch to epoch with the desired accuracy.

With the phase-delay technique, the differences between phase delays for two radio sources are used to determine their relative positions, because these differences have reduced sensitivity to unmodeled effects. For sources nearby to one another on the sky, this technique yields statistical standard errors of only a few microarcseconds (μas), as in the case of quasars 1038+528 A and B (Marcaide & Shapiro 1983; Marcaide et al. 1994), whose components are separated by only 33″. However, the overall standard errors are dominated by inaccuracies in the reference-point identification (e.g., Rioja et al. 1997). For sources with larger separations, the main contributions to the astrometric standard error in the relative position of two sources comes from uncertainties in the coordinates of the source chosen as the reference, in the value used for UT1–UTC, and in the effects of the propagation medium. For radio sources with separations ranging from 0.5° to 7° on the sky, standard errors in relative positions of about 0.1–0.3 mas have been obtained (Bartel et al. 1986; Guirado et al. 1995a,b, 1998; Lara et al. 1996; Ros et al. 1999).

A limiting factor in centimeter-wavelength VLBI astrometry is the uncertainty in the contribution of the ionosphere to the astrometric observables, even though its dispersive character makes this contribution scale as ν^{-2} and, in principle, allows it to be determined accurately (see,

Send offprint requests to: M.A. Pérez-Torres
⋆ *Present address:* Istituto di Radioastronomia, Via P. Gobetti 101, 40129 Bologna, Italy
Correspondence to: torres@ira.bo.cnr.it

e.g., Thompson et al. 1986). One strategy to take advantage of this scaling is to make simultaneous VLBI measurements in two frequency bands. The main disadvantage of this option is that the (fixed) bandwidth of the recording equipment has to be split between two frequency bands, decreasing the signal-to-noise-ratio (SNR) for each. Alternatively, one may compute corrections based on estimates of the ionosphere total electron content (TEC) obtained independently from Faraday-rotation measurements and, more recently, from the Global Positioning System (GPS). The advantage of the latter approach (e.g., Guirado et al. 1995b, Ros et al. 2000), is that only single-band VLBI observations are needed, avoiding the loss of sensitivity mentioned above.

In this paper, we study the applicability of the phase-difference technique to the strong radio sources 1150+812 and 1803+784, separated on the sky by almost 15°. We show that reliable phase connection is feasible at such a large angular separation, and estimate the relative position of the two sources with submilliarcsecond accuracy. We compare the estimates of the relative angular separation that result from use of two different methods of removing the ionosphere contribution based on two different types of data, namely, phase delays from dual-frequency-band VLBI measurements and TEC values from GPS measurements. The estimates from the two methods agree to within the standard errors from each method, showing that single-frequency astrometric VLBI experiments can be confidently carried out.

In Sect. 2, we briefly describe the observations; in Sect. 3 we describe the radio sources, and in Sect. 4 the data reduction process. In Sect. 5 we discuss our estimate of the relative position of the source 1803+784 with respect to 1150+812, and in Sect. 6 we carry out a sensitivity analysis of the estimated position of 1803+784 to errors in other model parameters. Finally, in Sect. 7 we summarize our main results and discuss their implications.

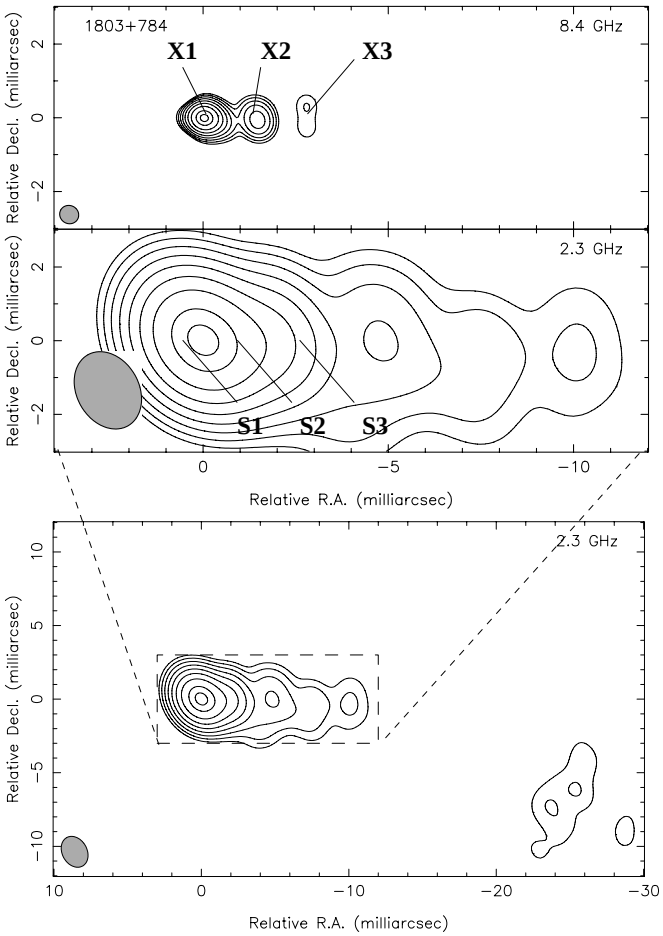

Fig. 1. Hybrid maps of 1803+784 at 8.4 (top) and 2.3 GHz (middle and bottom). Contours are 0.5,1,2,4,8,16,32,64, and 90% of the peaks of brightness, which are 1.48 Jy/beam and 1.35 Jy/beam for 8.4 and 2.3 GHz, respectively. The sizes of the restoring beams, shown shaded at the bottom left corners, are 0.52 × 0.49 mas (PA=61°) at 8.4 GHz and 2.21 × 1.68 mas (PA=29°) at 2.3 GHz. East is left, and north is up. The identification of the components in the 2.3 GHz map is based on an overresolved map (not shown here).

2. Observations

We observed the radio sources 1150+812 and 1803+784 on 18 November 1993 for 12 hours, in right circular polarization, simultaneously recording at two frequency bands (X-band ≈ 8.4 GHz and S-band ≈ 2.3 GHz). We used the following radio telescopes (in parenthesis we give the site symbol used in this paper, the diameter, and the location of the telecope): Effelsberg (B, 100 m, Germany); Medicina (L, 32 m, Italy); Onsala (S, 20 m, Sweden); Fort Davis (F, 25 m, Texas); Hancock (H, 25 m, New Hampshire); North Liberty (I, 25 m, Iowa); Owens Valley (O, 25 m, California); Los Alamos (X, 25 m, New Mexico); and the phased VLA (Y, 130 m equivalent, New Mexico). The European antennas (B, L, and S) recorded in Mark III mode A, covering a total bandwidth of 56 MHz, via seven adjacent channels spanning 8,403 to 8,431 MHz and seven such channels spanning 2,273 to 2,301 MHz. The American antennas used the Mark III recording system in mode B, covering a total bandwidth of 28 MHz, with four contiguous channels spanning 8,403 to 8,419 MHz and three such channels spanning 2,289 to 2,301 MHz. We used an observing cycle consisting of 2 min observing 1150+812, 1.5 min antenna slewing, 2 min observing 1803+784, and 1.5 min antenna slewing back to 1150+812, making a total cycle duration of 7 min.

The data were correlated at the MPIfR correlator in Bonn, Germany. Since both sources were strong (> 1 Jy) at the epoch of observation, we detected each of them with high SNR within the 2 min integration time, at both frequencies and for each baseline, except those baselines involving the Onsala antenna. After correlation, we exported the VLBI observables (fringe amplitude and phase,

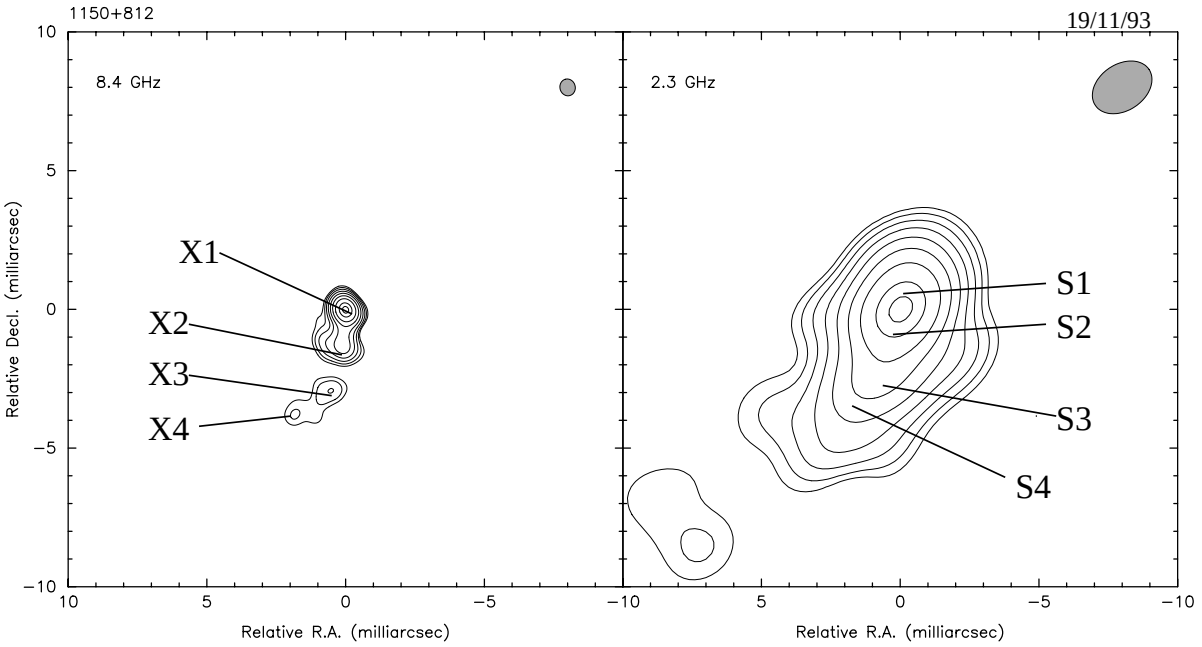

Fig. 2. Hybrid maps of 1150+812 at 8.4 (left) and 2.3 GHz (right). Contours are 0.5,1,2,4,8,16,32,64 and 90% of the peaks of brightness, which are 0.90 Jy/beam and 0.74 Jy/beam for 8.4 and 2.3 GHz, respectively. The sizes of the restoring beams, shown shaded at the upper right corners, are 0.61 × 0.55 mas (PA=15°) at 8.4 GHz and 2.33 × 1.67 mas (PA=-56°) at 2.3 GHz. The identification of the components in the 2.3 GHz map is based on an overresolved map (not shown here; see text).

group delay, and phase-delay rate) for the reference frequencies $\nu_{\rm X} = 8413$ MHz and $\nu_{\rm S} = 2295$ MHz, and calibrated the fringe amplitudes using the information provided by the staffs at the observing antennas. In our astrometric analysis, we discarded the data from Onsala due to the low SNR of the detections with this antenna; and from the phased VLA, since this antenna recorded only at 8.4 GHz and was used solely to increase the SNR of our hybrid maps. In addition, we discarded data from Effelsberg for the interval 18:30 until 23:28, since this antenna, too, only observed at 8.4 GHz during that interval. To obtain our hybrid maps, we self-calibrated, Fourier inverted, and CLEANed the visibility data using the Caltech program DIFMAP (Shepherd et al. 1995).

3. The Radio Sources

The radio source 1803+784 has been optically identified with a BL Lac object at z=0.684 (Stickel et al. 1991). This source has a nearly flat spectrum from millimeter to decimeter wavelengths (Strom & Biermann 1991) and displays many interesting properties (Biermann et al. 1981), including rapid variability, compactness, and strong X-ray emission.

Our 8.4 and 2.3 GHz maps of 1803+784 (Fig. 1) show a jet pointing westward. The hybrid map at 8.4 GHz shows the jet extending about 3 mas, with three components, labeled X1, X2, and X3. Most of the emission comes from components X1, identified as the core, and X2, about 1.5 mas west of X1. Component X3 lies about 2.8 mas west of X1 and is much fainter than X1 and X2. Our map at 2.3 GHz also shows the jet, which, as in the maps of Ros et al. (1999) and Eckart et al. (1987), extends up to about 25 mas and is slightly bent towards the southwest. At 2.3 GHz, most of the emission is concentrated within 3 mas of the peak, but emission is also discernible at points about 5, 8, and 10 mas west of S1 (Fig. 1, middle). These latter bright regions, especially the innermost and the outermost, may correspond to real features of the jet, but like the questionable features farther out, they are not relevant for our astrometric purposes and, therefore, are not labeled.

The radio source 1150+812 is a QSO with redshift $z = 1.25$ (Hewitt & Burbidge 1989). For this source, our 8.4 and 2.3 GHz maps (Fig. 2) indicate a curved jet directed to the south and west. The 8.4 GHz map contains at least four components, labeled X1 through X4, from north to south. Most of the emission comes from the components X1 and X2, which are separated by ~ 1.5 mas. Extended emission is still discernible at a distance of ~ 4 mas from X1 (components X3 and X4). At 2.3 GHz, the emission is concentrated within the innermost 5 mas, but emission is also evident farther to the southeast.

Our maps of 1803+784 and 1150+812 are in good agreement with maps of similar resolution from 1995 published by Fey & Charlot (1997).

4. Astrometric Data Reduction

Our strategy in the astrometric data analysis was to obtain a set of "connected" phase delays that could be analyzed via weighted-least-squares to estimate the relative position of the two sources.

The observables in our experiment, after correlating and fringe-fitting the data, were the interferometric phase, ϕ, the group delay, τ_G, and the phase-delay rate, $\dot{\tau}_\phi$. We based our analysis primarily on ϕ, converted first to the phase delay, τ_ϕ, via removal of the "$2\pi\,n$" ambiguities (where n is an integer). The delay equivalent of $2\,\pi$ in phase is ~ 120 ps at 8.4 GHz and ~ 440 ps at 2.3 GHz. To remove these ambiguities we used a "phase connection" technique (see, e.g., Shapiro et al. 1979) that can be outlined as follows: We constructed a model of the phase delays, based on a model of the geometry of our interferometric array and the radio sources (Table 1); the propagation medium; and the clock behavior at each station relative to a reference. We estimated the parameters of this model via weighted-least-squares analysis of the observed phase-delay rates and group delays. We used an improved version of the program VLBI3 (Robertson 1975) to carry out this weighted-least-squares analysis. The resultant model of the phase delays was accurate enough to allow phase connection, i.e., the elimination of the $2\pi\,n$ ambiguities for almost all of the observations (see below), via a suitable iterative scheme that took advantage of the closure relations over triangles of baselines. Since we phase-connected the data independently for each source, we used weighted-least-squares to verify – successfully – the consistency of the "overall resolution of ambiguities" of the delays for the two sources (see Ros et al. 1999 for a detailed discussion of this step). During our analysis, we discarded all data from the Hancock antenna, since our phase connection failed at both frequencies. We also discarded the data from the Medicina antenna from 18:30 to 23:48, since in this time period our phase-connection appeared to be unreliable. (These failures are likely the result of some combination of tropospheric, ionospheric, and instrumental effects.)

4.1. Source-Structure Contribution

The extended structure of even a "compact" radio source often makes a significant contribution to the phase delays. Such a contribution depends on the point chosen as a reference on the map. Identifying a reference point in a reliably epoch-independent manner is crucial for the use of our method to compare positions obtained from different epochs. For each source and frequency band, our procedure was to choose the peak of brightness (POB) as the reference point. To find the POB, we constructed fine-grained maps of the two radio sources using pixel size 0.01 mas at 8.4 GHz and 0.03 mas at 2.3 GHz. We identified the brightest pixel in each such map as the POB and defined a new coordinate system with that reference point as its origin. We then computed from these maps the structure-phase contribution to each phase delay. These contributions – up to ~ 25 ps at 8.4 GHz and ~ 55 ps at 2.3 GHz – were removed from the phase delays, to effect a point-like source at each POB. The standard deviations assigned to each POB location included uncertainties due to (a) the pixel size used for each map, which was about 0.01 (0.03) mas at 8.4 (2.3) GHz, for each source; and (b) SNR for the peak, which was about 0.04 (0.27) mas at 8.4 (2.3) GHz, for each source. Note, however, that when the delays at the two frequencies are combined to form "plasma-free" delays, errors in the phase delays at 2.3 GHz are scaled down by a factor $[(\nu_X/\nu_S)^2 - 1]^{-1} \approx 0.08$ (see Sect. 4.4), and therefore the uncertainty of the POB at 2.3 GHz is less significant than that of the POB at 8.4 GHz. The root-sum-squares of these contributions, at each frequency, are indicated as the first (8.4 GHz) and second (2.3 GHz) entries in Table 2, and are dominated by the relatively low SNR of the hybrid maps.

4.2. Neutral Atmosphere Contribution

The neutral atmosphere (primarily the troposphere) adds an extra delay to the incoming radio waves, the equivalent of up to a few meters in pathlength. We monitored the pressure, relative humidity, and temperature at each observing antenna to track the atmosphere behavior during the observations. We used the model by Saastamoinen 1993, in which the atmosphere is separated into two components: a dry component and a wet component (due to the water vapor in the atmosphere). Based on this model, we calculated a priori values for the delays for the wet and dry atmosphere components in the zenith direction for each antenna site (Table 1), and then used the Chao (1974) mapping function to determine delays at other elevations. This mapping function agrees to within about 1 cm with ray-tracing computations (Davis et al. 1985) for antenna elevations larger than 20°; all of our observations had elevation angles above this limit. To specify adjustments to the combined (dry and wet) atmosphere delays during the observations, we used a piecewise-linear function characterized by zenith delay values at epochs about three hours apart. Errors in the combined neutral-atmosphere delays – mainly due to the wet troposphere – are likely to be up to 0.1 ns/hr (D. Lebach, priv. comm.). Since the wet atmosphere zenith delay fluctuates approximately as a random walk (Treuhaft & Lanyi 1987), an error of 0.1 ns/hr transforms into a standard error of $\sqrt{3} \times 0.1 \approx 0.17$ ns every three hours. Therefore, in our sensitivity analysis, we allowed the atmosphere parameters at each antenna location to vary with this standard error.

Table 1. A priori values of the parameters of the theoretical model used in the estimates of the source positions

Source coordinates (J2000.0)[a]

1150+812	$\alpha = 11^h53^m12^s.499188$	$\delta = 80°58'29''.15453$
1803+784[b]	$\alpha = 18^h00^m45^s.683922$	$\delta = 78°28'04''.01852$

Antenna site coordinates and atmosphere parameters

Radio telescopes[a]		Cartesian coordinates [m] X	Y	Z	Axis offset [m]	Mean atmosphere zenith delay[c] [ns] $\tau_{\rm dry}$	$\tau_{\rm wet}$
B	Effelsberg	4033947.51	486990.46	4900430.75	0.00	7.5	0.1
F	Fort Davis	–1324009.08	–5332181.98	3231962.49	2.12	6.4	0.1
I	North Liberty	–130872.19	–4762317.13	4226851.05	2.13	7.5	0.1
L	Medicina	4461370.05	919596.77	4449559.16	1.83	7.7	0.2
O	Owens Valley	–2409150.05	–4478573.27	3838617.42	2.13	6.8	0.1
X	Los Alamos	–1449752.31	–4975298.60	3709123.95	2.14	6.2	0.1

Earth Tides

Radial Love number[d], $\mathbf{h} = 0.60967$ Tidal lag angle, $\theta = 0°.0$

Horizontal Love number[d], $\mathbf{l} = 0.085$

Precession Constant (J2000.0)[e]
$\mathbf{p}$=5029″.0966/Julian Century
Mean obliquity (J2000.0)[e]
ϵ_0=23°26′21″.448=84381″.448

Polar Motion and UT1
Interpolated from daily values from IERS (1996)

Nutation
Interpolation of IAU 1980 Nutation Model with IERS (1996) daily corrections

[a] We took 0.058 ms and 0.140 mas to be the standard errors in the right ascension and declination, respectively, of 1150+812, twice the quoted IERS (1996) errors. We also used as standard errors 2 cm in each coordinate of every antenna location (conservatively chosen to be at least twofold larger than the errors given by IERS), 0.7 mas in each pole coordinate, and 0.04 ms in UT1–UTC. We calculated the location of each antenna by linear extrapolation, using the velocity given by the IERS, and applied to the 1993.0 position, also given by the IERS. coordinates obtained from IERS and applied to its 1993.0 positions.

[b] The coordinates of 1803+784 serve only as an initial estimate, and do not affect our results.

[c] Mean values of sampled zenith delays, computed using the meteorological values provided by the staff at the observing antennas.

[d] Dahlen (1976).

[e] Lieske et al. (1977).

4.3. Ionosphere Contribution

As explained in Sect. 1, we removed most of the ionosphere contribution in two alternative ways, first by using our dual-frequency-band observations and, second, by using the total electron content (TEC) values deduced from GPS measurements (see, e.g., Sardón et al. 1994). For the latter removal, we followed the same procedure as described in Ros et al. (2000), modeling the ionosphere as a thin layer located at an altitude of 350 km. We used GPS data from Wettzell (Germany) to obtain TEC values for Effelsberg and Medicina, and from Goldstone (California) to obtain TEC values for Owens Valley, Los Alamos, and Fort Davis; we were fortunate to have a GPS antenna collocated with our VLBI antenna at North Liberty to obtain TEC values for this site. In Fig. 3 we compare the estimated ionosphere delays as deduced from both dual-frequency-band observations (8.4 GHz/2.3 GHz delays) and GPS-based measurements (TEC delays), for a representative subset of baselines, intracontinental (upper two plots) and intercontinental (lower two plots). Dual-frequency corrections refer only to baselines, not individual antennas. On the other hand, TEC ionosphere corrections are calculated for individual antennas. Therefore, for each antenna there can be a constant offset between the TEC ionosphere correction and the dual-frequency one as a result of instrumental effects, but, for clarity, we subtracted the mean difference between each of the two corrections (Effelsberg, 1.35 ns; Medicina, 0.55 ns; North Liberty, 7.80 ns; Fort Davis and Los Alamos had no offset). We assumed a statistical standard error for the vertical TEC at each GPS antenna of $2 \times 10^{16}\,{\rm m}^{-2}$ (Sardón, priv. comm.), corresponding to a standard error of $\sim$40 ps for the (vertical) phase delays at 8.4 GHz. For each antenna, this error is multiplied by the value from the mapping function for the elevation angle of each radio source (here, the secant of the zenith angle at the ionospheric point) of each radio source. The resultant mapped TEC-based ionosphere corrections had standard errors ranging from $\sim$ 70 ps to $\sim$ 120 ps (Fig. 3). The standard errors for our dual-frequency-band corrections are the appropriate combination of the statistical errors of the phase delays at each frequency, and ranged from $\sim$5 ps for the Effelsberg–Medicina baseline up to $\sim$30 ps for the Fort Davis–Owens Valley baseline. The root-mean-square (rms) of the differences between the corrections obtained by the two methods ranged from $\sim$ 20 ps up to $\sim$ 90 ps, depending on baseline. The maximum difference was for intercontinental baselines and was $\sim$ 110 ps, when it was night in Europe and noon in North America. The level of agreement in the results from the two methods is gratifying, and fore-

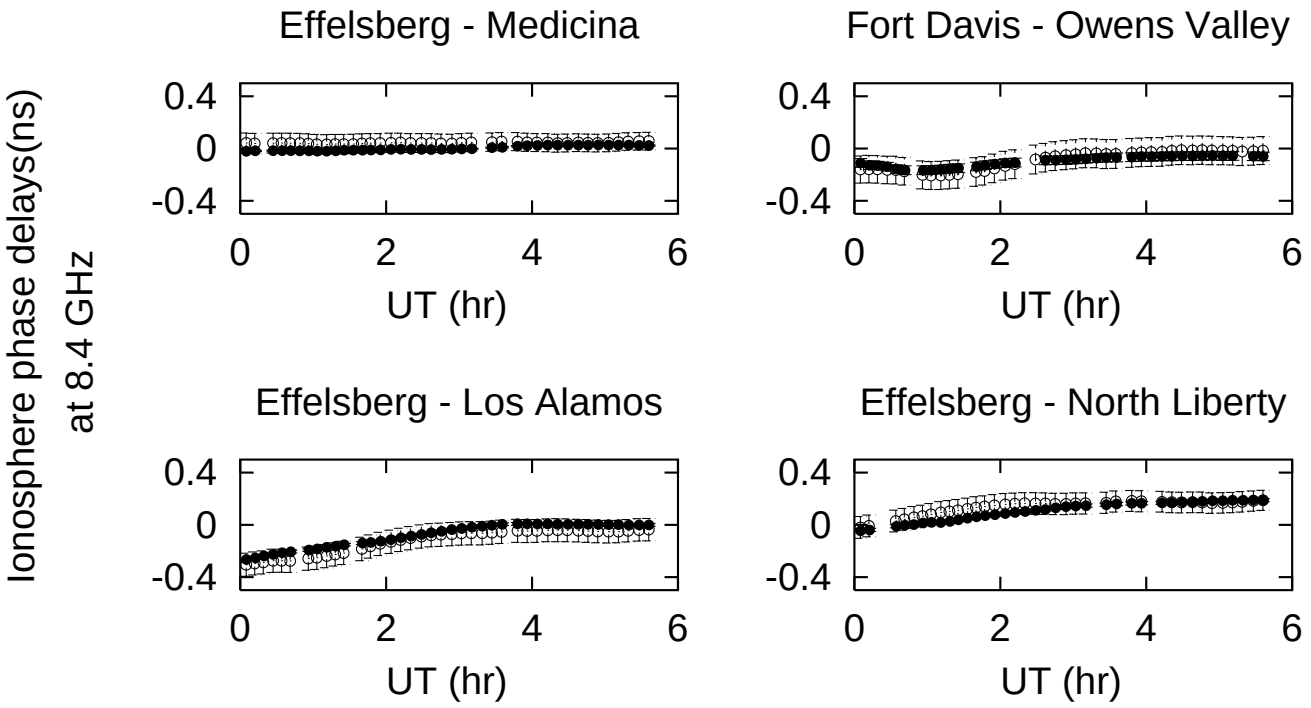

Fig. 3. Ionosphere contribution, in nsec at 8.4 GHz, as obtained from our dual-frequency-band (8.4/2.3 GHz) measurements (filled circles) and from the GPS-based measurements (open circles), for a representative set of baselines including both intracontinental and intercontinental baselines. The standard errors shown are for the TEC-inferred delays, and are much larger than those from dual-frequency-band measurements. All four plots start at 00:00, since until approximately that time Effelsberg observed only at 8.4 GHz, and thus lacked dual-frequency-band corrections.

shadows the agreement in the astrometric results obtained below with the two methods.

4.4. Opacity Contribution

When we use phase delays at both 8.4 and 2.3 GHz (see Sect. 4.3), the reference points on the 2.3 GHz maps should be chosen to correspond to the same points in the sky as those on the 8.4 GHz maps. Unfortunately, opacity effects may introduce an offset between the POB for one frequency band with respect to the POB for the other frequency band (see, e.g., Marcaide & Shapiro 1984). Since jet components are less self-absorbed than core components, their associated peaks should be less affected by opacity effects and should therefore be better suited for use as guides for the alignment of the maps at 8.4 and 2.3 GHz. We registered the peaks of the less self-absorbed components in our 8.4 GHz maps with their corresponding peaks in (twofold overresolved) 2.3 GHz maps.

For 1803+784, we identified component X3 at 8.4 GHz with component S3 at 2.3 GHz (Fig. 1) on a twofold overresolved map (not shown). Based on this map, we concluded that blended components S1, S2, and S3 at 2.3 GHz correspond to components X1, X2, and X3, respectively, in the 8.4 GHz map. This identification implied that in our maps the POB of 1803+784 at 2.3 GHz (S1) is offset by ~ 0.6 mas westward from the POB at 8.4 GHz (X1). For 1150+812, we also used a twofold overresolved map at 2.3 GHz to make a plausible registration of the maps for the two bands. We identified components X3 and X4 at 8.4 GHz with components S3 and S4 at 2.3 GHz (Fig. 2), implying a shift of the POB at 2.3 GHz (S1) of ~ 0.5 mas northward from the peak of the core in the 8.4 GHz map (X1). To estimate the standard error in our determination of those shifts we followed a similar procedure to that described for the determination of the standard error associated with the reference-point identification (POB), but applied to components X3 and S3, for each source. This procedure yielded an standard error of 0.4 mas for each source. Finally, to take into account the possible additional shifts due to opacity effects of the POB of component S3 with respect to X3, for each source, we increased the estimated standard error in each coordinate of the registration estimate from 0.4 mas to 0.7 mas. Estimates of the shift between the POBs at 8.4 and 2.3 GHz (where opacity effects are expected to be larger than in the jet components) of other radio sources – 1038+528 A (Marcaide & Shapiro 1984), 1226+023 (Charlot 1993), 1901+319 (Lara et al. 1994) – are also no greater than 0.7 mas. Thus, our estimates of these shifts for 1803+784 and 1150+812 seem reasonable.

In this dual-frequency-band method to reduce the ionosphere contribution, the resultant "ionosphere-free" phase delays have the form:

$$\tau_{\phi,free} = \frac{R\,\tau_{\phi,1} - \tau_{\phi,2}}{R-1}$$

where the subscripts 1 and 2 refer to the two frequency bands, with $\nu_1 > \nu_2$ and $R = (\nu_1/\nu_2)^2$. In our case, $R \simeq (8.4/2.3)^2 \simeq 13$; hence standard errors in the phase delays at 8.4 GHz are scaled up by a factor $R/(R-1) \simeq 1.08$, whereas corresponding errors in the phase delays at 2.3 GHz are scaled down by $1/(R-1) \simeq 0.08$ in their effect on $\tau_{\phi,\rm free}$. Likewise, uncertainties accounting for registration errors due to opacity effects have to be scaled by $1/(R-1)$. Thus, the contribution to the total error budget due to the use of dual-frequency-band measurements, in particular the seemingly large error at 2.3 GHz discussed above, is not significant (see entry "Opacity effects" in Table 2).

Table 2. Contributions to the standard errors of the estimates of the relative coordinates of the POB at 8.4 GHz of 1150+812 and 1803+784

Effect	$\sigma_{\Delta\alpha}$ [a] mas	$\sigma_{\Delta\delta}$ [a] mas
8.4 GHz source structure[b]	0.07	0.07
2.3 GHz source structure[c]	0.04	0.04
Opacity effects[c]	0.08	0.08
Statistical errors[d]	0.41	0.62
Software limitations[e]	0.40	0.40
Root-sum-square	0.58	0.75

[a] Contributions to the standard errors of the estimates of the coordinates of 1803+784 minus those of 1150+812, namely relative right ascension, $\Delta\alpha$, and relative declination, $\Delta\delta$.
[b] Root-sum-square (rss) of the standard errors due to the use of data at 8.4 GHz. Each value has been scaled by $R/(R-1) \approx 1.08$. See Sect. 4.4.
[c] rss of the standard errors due to the use of data at 2.3 GHz, which includes estimated errors in the "registration" of the 2.3 GHz and 8.4 GHz maps, taken to be 0.7 mas for each source. Each value has been scaled by $1/(R-1) \approx 0.08$. See Sect. 4.4.
[d] We estimated $\sigma_{\Delta\alpha}$ in milliseconds (ms). To transform this estimate into milliarcseconds (mas), we multiplied by $15 \cdot \cos\delta_{1803+784}$.
[e] See Sect. 6.

5. Relative Position of the Two Sources

We obtained a final set of phase delays for each source by correcting for source-structure, opacity-effect, and ionosphere contributions as described above. We then formed a set of differenced phase delays by subtracting the delay for each observation of 1803+784 from the corresponding delay for the previous observation of 1150+812. The use of differenced phase delays is in general more effective the closer together are the sources in the sky, since differencing results from neighboring observations tends to cancel effects which for each source alone cannot be accurately enough described by theoretical models. The best such pair of sources for such cancellation so far studied is 1038+528 A and B (Marcaide & Shapiro 1983), because this pair simultaneously lies inside the beam of each antenna, yielding almost complete cancellation of several sources of error. For sources separated by increasingly larger angular distances, the cancellation of unmodeled effects in general lessens, due directly to the increase in angular separation of the sources and indirectly to the increase of the cycle length of the observations.

From a weighted-least-squares analysis of the differenced phase delays, we estimated the coordinates of 1803+784 relative to those of 1150+812 (see Table 3). In this analysis, we also included the (undifferenced) phase delays of 1150+812, suitably weighted, to estimate the relative behavior of the site clocks. (The opposite scheme, i.e., using the differenced phase delays of 1803+784 minus those for 1150+812, and the undifferenced phase delays of 1803+784, did not alter significantly our estimate.) The total number of parameters whose values were estimated was 26, and include those of a third-degree polynomial to model the clock behavior at each station (except for North Liberty, which was taken as our reference station), the coordinates of 1803+784, and four atmosphere parameters (see Sect. 4.2) for the Effelsberg antenna, since the information on the atmosphere conditions provided for this site was very sparse, and thus of doubtful utility. Nonetheless, the estimated atmosphere parameters for Effelsberg agreed with the a priori values within 0.11 ns.

Our choice of 1150+812 as the reference source was motivated by its being one of the defining sources of the quasi-inertial International Celestial Reference Frame. As a test of the effect of this choice, we solved for the coordinates of 1150+812–keeping those of 1803+784 fixed at their IERS values–and obtained different results for $\Delta\alpha$ and $\Delta\delta$. As a simple check on the significance of those differences – one that avoids the effects of the reference system in which the coordinates are expressed – we calculated the arclength between the two sources for each of the two solutions. We expected to obtain nearly the same result for the two cases and indeed, the difference was a mere 5 μas, negligible compared to the overall standard errors of our results.

For our nominal, dual-frequency-band solution described above, we scaled separately the standard deviations of the differenced phase delays and of the phase delays of 1803+784, so that for the data for each type, and for each baseline, the weighted-mean-square of the post-fit residuals was nearly unity. As a result, the error bars assigned to the differenced phase delays were, in general, smaller by a factor ~ 1.2 with respect to the error bars assigned to the phase delays of 1150+812 (see Figs. 4 and 5). We studied the effect of varying the relative weights of our two data types and verified that such variations did not change our result significantly. In fact, any ra-

Table 3. Phase-delay-based estimates of the coordinates of 1803+784 minus those of 1150+812

	Ionosphere correction method	
	Dual-frequency [a] (mas)	GPS-derived TEC [b] (mas)
$\Delta\alpha - 6^h\,7^m\,33\overset{s}{.}18473$[c]	-0.12 ± 0.58[d]	$+0.12 \pm 0.78$[d]
$\Delta\delta + 2^\circ\,30'\,25\overset{''}{.}13601$[c]	-0.44 ± 0.75	-0.31 ± 0.82

[a] Estimates of the relative position of the two sources, minus the reference separation, from a weighted-least-squares analysis of the phase delays, after corrections for source-structure, source opacity, and ionosphere effects, the last via dual-frequency-band observations. The estimated standard errors include statistical standard errors and errors due to opacity effects, to registration of the maps, and to software limitations. See Table 2 and Sect. 6.

[b] Estimates of the same relative position as above, except that only phase delays at 8.4 GHz were used and that the corrections for ionosphere effects were obtained from GPS-based estimates of TEC.

[c] The reference separations are from the IERS (1996). See Table 1.

[d] To facilitate comparisons between $\Delta\alpha$ and $\Delta\delta$, we have multiplied the $\Delta\alpha$ (ms) values by $15 \cdot \cos\delta_{1803+784}$ to obtain $\Delta\alpha$ in mas.

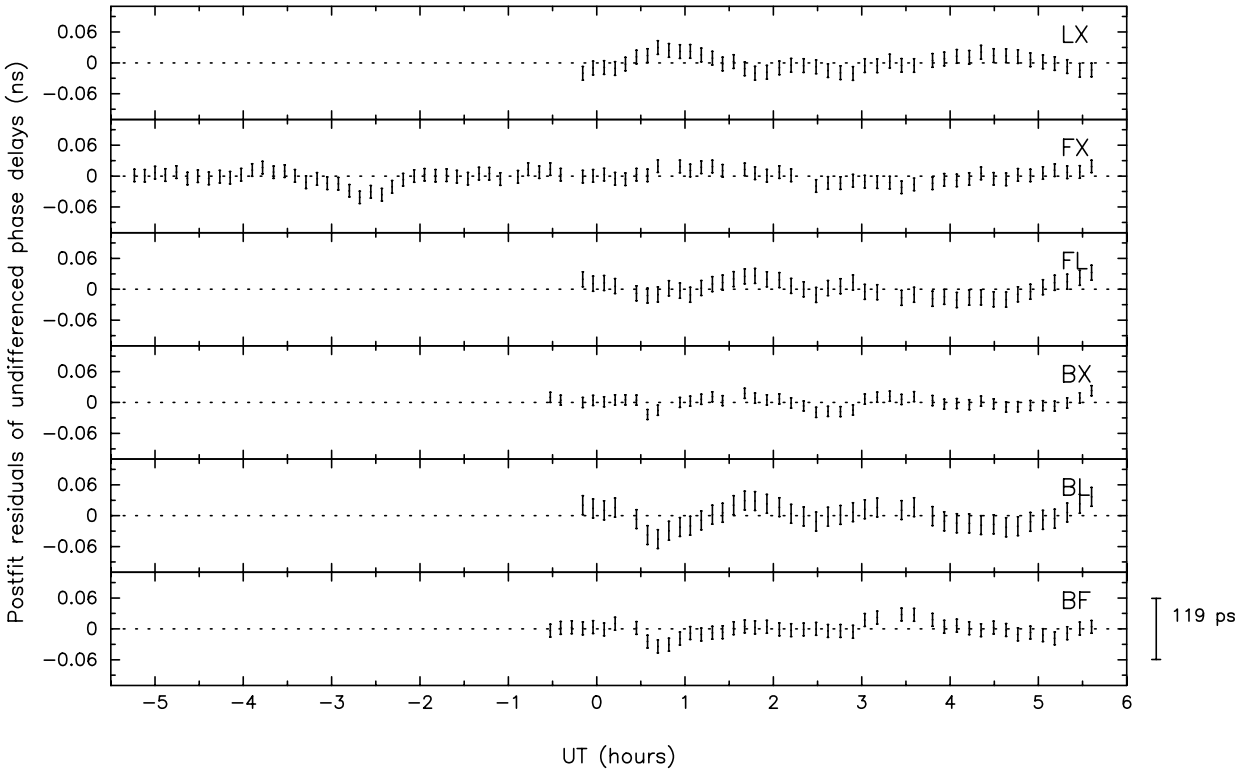

Fig. 4. Postfit residuals of the phase delays (ns) of 1150+812 for the subset of baselines involving the following antennas: Effelsberg (B), Medicina (L), Fort Davis (F), and Los Alamos (X). The solution utilized corrections for ionosphere effects determined from our dual-frequency-band observations. For that reason, the baselines involving Effelsberg show a large time gap, since this antenna observed in dual-frequency mode after 23:28. Similarly, the Medicina antenna shows a gap until 23:48, since the phase-delay connection for this antenna appeared uncertain in this time range. One ambiguity interval at 8.4 GHz is 119 ps (shown at the right margin). The error bars shown are the standard deviations of the phase delays, scaled so that the weighted-mean-square of the postfit residuals is unity for each baseline (see text).

tio of the weights of the differenced to the undifferenced data between 0.1 and 10 with respect to our "nominal" solution did not alter our estimate of the angular separation significantly. Figs. 4 and 5 also illustrate a virtue of the difference phase-delay technique mentioned above: although the separation of the sources is $14^\circ\,50'\,21\overset{''}{.}147559$ and the cycle length of the observations is correspondingly large, the differenced phase delays are partially free from some incompletely modeled effects as attested by the larger residuals seen in Fig. 4 than in Fig. 5, in particular for the baselines involving the Medicina antenna.

The standard errors in Table 3 are larger than the differences between our estimates of $\Delta\alpha$ and $\Delta\delta$, and those provided by IERS, indicating that the a priori IERS values

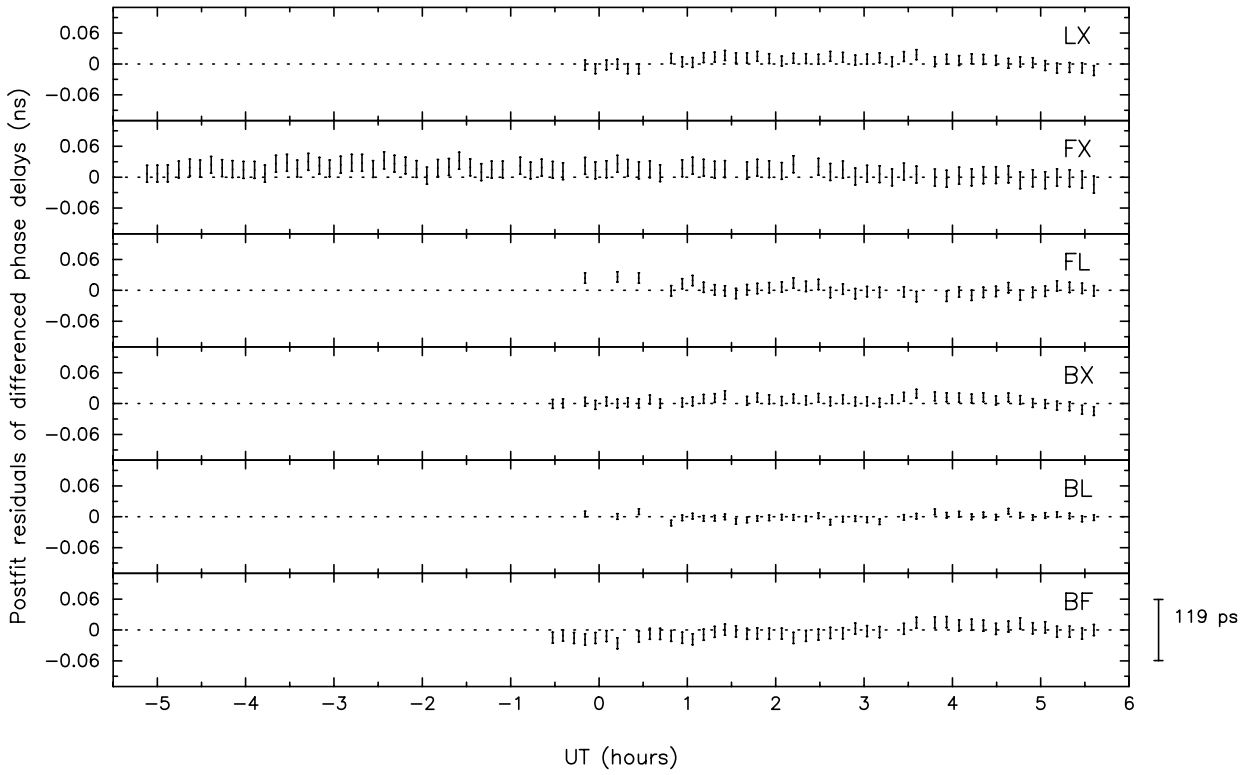

Fig. 5. Postfit residuals of differenced phase delays (ns) for the same solution and the same subset of baselines as in Fig. 4. The error bars shown are the standard deviations of the differenced phase delays, scaled so that the weighted-mean-square of the postfit residuals is unity for each baseline (see text).

are quite accurate. This accuracy is not surprising, since both radio sources are dominated by emission from the core, and so the IERS values – mainly based on averages of results from observations at many epochs using group-delay astrometry – should be accurate, except for a small offset that may be contributed by persistent opacity effects in the core components. For sources with strong emitting features well separated from their cores, larger differences from the a priori IERS values can be expected, given the greater sensitivity of the "structure group delay" to components farther from the cores (Thomas 1980). Those differences can be largely removed by using the more precise, structure-free phase delays.

6. Sensitivity Analysis

We carried out a sensitivity analysis to estimate the contributions of individual effects to the standard errors in the relative-position determination; see Table 4 for a list of these effects. We found that the primary source of error is due to the uncertainty in our knowledge of the neutral atmosphere, which by itself contributes a standard error of about 0.4 mas in right ascension and about 0.6 mas in declination to the estimate of the position of 1803+784. To be conservative in our estimate of the error contributed by the neutral atmosphere, we took for each site the larger of the following two values: the root-sum-square of the delay contribution from all atmosphere parameters for that site (one every three hours), or the algebraic sum of the signed partials. In this way, we made some allowance for the potential effects of possible correlations among the estimates of the atmosphere parameters for each site. The second largest contribution to the total error budget of each coordinate comes from the corresponding standard error in the a priori position used for the reference source (1150+812). This large contribution is due to the geometry of the sources on the sky. For sources with smaller angular separations, the contribution of the a priori uncertainties of the coordinates of the reference source to the standard error in relative position is usually a small fraction of the a priori uncertainty of the reference coordinates (e.g., Guirado et al. 1995b), because there is a positive correlation between the right ascensions, and similarly the declinations, of the two sources. However, because 1150+812 and 1803+784 are within 12° of the north celestial pole and lie almost exactly six hours apart in right ascension, an error in the position of one of the sources in right ascension (or declination) translates into a similar error for the other source in declination (or right ascension). (See Table 4.) A covariance analysis confirms this "tradeoff", showing a fairly strong correlation between the estimates of the right ascension of one source and the

declination of the other source ($\rho(\alpha_{1150+812}, \delta_{1803+784}) \approx -0.7; \rho(\delta_{1150+812}, \alpha_{1803+784}) \approx 0.7$), but little correlation between the estimates of the two right ascensions (and between the two declinations). Moreover, the nearly complete cancellation of the geometric errors usually obtained in astrometric studies of radio sources with smaller angular separations is not so effective in the present case. For example, the uncertainties in UT1–UTC values do contribute significantly to the standard error in the estimate of the angular separation. The remaining significant contributions to the standard error are attributable to the uncertainties in the estimates of the antenna locations.

Table 4. Sensitivity of the estimated position of 1803+784 to the values of other model parameters included in the weighted-least-squares analysis.

Parameter		Standard Deviation[a]	$\delta\Delta\alpha$ (μas)[b]	$\delta\Delta\delta$ (μas)
$\alpha_{1150+812}$[c]		174 μas	–6	–158
$\delta_{1150+812}$[c]		140 μas	135	–2
Atmosphere	F	0.17 ns/3 hr	–123	298
zenith delays[d]:	I	0.17 ns/3 hr	–150	–87
	L	0.17 ns/3 hr	–267	117
	O	0.17 ns/3 hr	111	415
	X	0.17 ns/3 hr	–45	227
Site coordinates[e]:	B	2 cm	60	40
	F	2 cm	30	35
	I	2 cm	42	20
	L	2 cm	69	32
	O	2 cm	34	76
	X	2 cm	24	39
Earth's pole[c]:	x	0.7 mas	18	–1
	y	0.7 mas	8	21
UT1–UTC[c]		0.04 ms	-126	-95
Root-Sum-Square			**412**	**616**

[a] Each value in the $\delta\Delta\alpha$ and $\delta\Delta\delta$ columns was obtained by computing the effect of altering the a priori value of each parameter by one standard deviation on the relative-position determination.

[b] We have multiplied μs by $15 \cdot \cos\delta_{1803+784}$ to obtain μas for the penultimate column.

[c] The standard deviations are as provided in IERS (1996). For the sensitivity analysis, we adopted standard deviations for the coordinates of 1150+812 twofold the quoted IERS (1996) errors.

[d] We specified the atmosphere delays at each site by a piecewise-linear function characterized by values at epochs about three hours apart. For each such epoch, we used 0.17 ns as the standard error. The quoted sensitivity values take into account the total contribution, for each antenna, from all atmosphere parameters. Effelsberg (B) is not included, since we solved for its atmosphere parameters. (See Sect. 4.2).

[e] As given in Table 1. The 2 cm standard deviation refers to each of the three coordinates for each antenna site. The sensitivity values account for the errors in all three coordinates, assumed to be independent.

Software limitations prevented us from taking into account in our analysis such effects as ocean and atmosphere loading, tidal terms in polar motion and UT1, and arbitrary variations in the atmosphere zenith delays. Based upong a surrogate test of the sensitivity of the relative position of a different pair of radio sources (observed in an unrelated experiment) to these effects, performed using the CALC (Ma et al. 1986) and SOLVK (Herring et al. 1990) packages, we estimated that the known limitations of our software contribute an uncertainty of about 0.4 mas to each coordinate of our estimate of the sources' relative position.

7. Summary

We observed the strong radio sources 1150+812 and 1803+784 with a VLBI array on 18 November 1993, an epoch of mild solar activity. The antennas recorded data simultaneously at 8.4 and 2.3 GHz, which allowed us to estimate the ionosphere contributions to the phase delays; we also used TEC values from GPS measurements to estimate such contributions. We estimated, and thereby partly removed from the phase-delay data, contributions due to the dry and wet components of the atmosphere, and the brightness structure of the sources. The phase-connection process, required to extract the precision inherent in the phase delays, did not pose special difficulties for our 7 min cycle time, indicating that spatial and temporal fluctuations due to the atmosphere and the ionosphere were not large enough to prevent reliable phase connection in either frequency band.

We then estimated the relative position of the sources (Table 3) via a weighted-least-squares analysis of a combined data set of undifferenced and differenced phase delays. The estimates resulting from use of GPS-based TEC values to account for ionosphere effects agree with those obtained from our dual-frequency-band VLBI measurements to within the standard errors for each method. Ros et al. (1999, 2000) also successfully used GPS-based TEC values to remove the ionosphere's contribution to the phase delays at 8.4 GHz. The checking of their removal in that experiment was limited to the precision of the dual-frequency-band (8.4 and 2.3 GHz) group delays, since Ros et al. could not reliably connect their phase delays at 2.3 GHz. In our case, we successfully connected the phase delays at both frequencies, and thus for the first time compared TEC ionosphere delays against phase-delay-based ionosphere corrections (Fig. 3). This agreement supports the use of single-band ($\geq$ 8.4 GHz) VLBI observations for astrometry purposes, an option of particular interest for experiments to be carried out at epochs of strong solar activity, when phase connection for a frequency band $\leq$ 2.3 GHz is likely to fail. Single-frequency VLBI observations along with GPS-derived TEC ionosphere corrections can be confidently used instead.

Our standard errors shown in Table 3 are larger than the difference between our estimates of relative source position and those provided by IERS. The high level of agreement is likely due to the fact that both radio sources are strongly core-dominated. However, were a bright emitting feature present several milliarcseconds from one of the cores, large offsets could exist between the true core position and the IERS position. With VLBI phase-delay astrometry, such errors can be effectively reduced using structure-phase corrections computed from self-calibrated maps derived from the same VLBI observations. Moreover, phase-delay astrometry has the advantage of allowing us to know *very* accurately to which feature *inside* each source we are referring when calculating relative positions.

In summary, we have determined with submilliarcsecond accuracy the angular separation of two radio sources separated by almost 15°, using phase delays from dual-frequency-band VLBI measurements. Since within 15° of any given source there are almost always two or more reasonably strong radio sources, we have thus demonstrated that phase delays should be usable for full-sky astrometry of radio sources, We have also shown that GPS-based measurements can be used to obtain reliable ionosphere corrections to the phase delays, thus demonstrating the feasibility of conducting VLBI solely observations at frequencies ≥ 8.4 GHz for astrometric purposes. Future improvements in the modeling of the atmospheric delay contribution, and in the knowledge of Earth rotation and pole position, as well as antenna location, should result in increasingly accurate estimates of the relative positions of sources far apart on the sky.

We stress that phase delays are more reliably corrected for structure phase than are group delays. Therefore, differenced phase-delay astrometry is better suited than group-delay astrometry for carrying out astrometric studies of extended radio sources. To date, however, group-delay astrometry has been used to establish a quasi-inertial celestial reference frame based on estimates of the positions of a number of relatively compact extragalactic radio sources from many years of regular observations. Our results open the avenue to an alternative, potentially more accurate, approach, namely that of carrying out a suitable series of observing sessions and using difference phase-delay astrometry to obtain submilliarcsecond positions for the cores of these sources.

Acknowledgements. We are grateful to the referee, Jim Ulvestad, for valuable comments and suggestions. We thank the staffs of all the observatories for their contribution to the observations, and in particular the MPIfR staff for their efforts during the correlation. We also thank Dan Lebach for his work with the CALC/SOLVK package to test the quantitative significance of the limitations of our VLBI3 program. This work has been partially supported by the Spanish DGICYT grants PB93-0030 and PB96-0782, and by the European Comission's TMR-LSF program under contract No. ERBFMGECT950012. The VLA is a facility of the National Radio Astronomy Observatory. The NRAO is a facility of the National Science Foundation operated under cooperative agreement by Associated Universities, Inc.

References

Bartel N., Herring T.A., Ratner M.I., et al., 1986, Nat 319, 733
Biermann P., Duerbeck H., Eckart A., et al., 1981, ApJ 247, L53
Chao C.C., 1974, JPL/NASA Tech. Rep. No. 32-1587, 61
Charlot P., 1993, The spectral indices of the parsec-scale jet components of 3C 273. In: Davis R., Booth R.S. (eds.), Subarcsecond Radioastronomy. Cambridge University Press, Cambridge, p. 218
Dahlen F.A., 1976, Geophys. J. Roy. Astr. Soc. 46, 363
Davis J.L., Herring T.A., Shapiro I.I., et al., 1985, Radio Science 20, 1593
Eckart A., Witzel A., Biermann P., et al., 1987, A&AS 67, 121
Fey A.L., Charlot P., 1997, ApJS 111, 95
Guirado J.C., Marcaide J.M., Alberdi, A., et al., 1995b, AJ 110, 2586
Guirado J.C., Marcaide J.M., Elósegui P., et al., 1995a, A&A 293, 613
Guirado J.C., Marcaide J.M., Ros E., et al., 1998, A&A 336, 385
Hewitt A., Burbidge G., 1993, ApJS 87, 451
Herring T.A., Davis J.L., Shapiro I.I., 1990, J. Geophys. Res. 95, 12561
International Earth Rotation Service (IERS) 1996, Annual Report for 1995. Feissel M., Essaïfi N. (eds.), Paris
Lara L., Marcaide J.M., Alberdi A., et al., 1994, A&A 285, 393
Lara L., Marcaide J.M., Alberdi A., Guirado J.C., 1996, A&A 314, 672
Lieske J.H., Lederle T., Fricke W., 1977, A&A 58, 1
Ma C., Clark T.A., Ryan J.W., et al., 1986, AJ 92, 1020
Ma C., Arias E.F., Eubanks T.M., et al., 1998, ApJ 116, 516
Marcaide J.M., Shapiro I.I., 1983, AJ 88, 1133
Marcaide J.M., Shapiro I.I., 1984, ApJ 276, 56
Marcaide J.M., Elósegui P., Shapiro I.I., 1994, AJ 108, 368
Rioja M.J., Marcaide J.M., Elósegui P., et al., 1997, A&A 325, 383
Robertson D.S., 1975, Ph.D. Thesis, Massachusetts Institute of Technology
Ros E., Marcaide J.M., Guirado J.C., et al., 1999, A&A 348, 381
Ros E., Marcaide J.M., Guirado J.C., et al., 2000, A&A, 356, 357
Saastamoinen J., 1973, Bull. Géodésique 105, 279
Sardón E., Rius A., Zarraoa N. 1994, Radio Science 29, 577
Shapiro I.I., Wittels J.J., Counselman C.C., et al., 1979, AJ 84, 1459
Shepherd M.C., Pearson T.J., Taylor G.B. 1995, BAAS 26, 987
Stickel M., Fried J.W., Kühr H., et al., 1991, ApJ 374, 431
Strom R.G., Biermann P.L., 1991, A&A 242, 313
Thomas J.B., 1980, An analysis of Source Structure Effects in Radio Interferometry Measurements, JPL Publication 80-84, Jet Propulsion Laboratory
Thompson A.R., Moran J.M., Swenson G.W., 1986, Interferometry and Synthesis in Radio Astronomy. Wiley, New York
Treuhaft R.N., Lanyi G.E., 1987, Radio Science 22, 251